PCCP

ROYAL SOCIETY OF CHEMISTRY

PAPER

View Article Online
View Journal | View Issue

Cite this: *Phys. Chem. Chem. Phys.*, 2022, **24**, 20409

A computational tool to accurately and quickly predict ^{19}F NMR chemical shifts of molecules with fluorine–carbon and fluorine–boron bonds

Alexandre S. Dumon, [a] Henry S. Rzepa, *[a] Carla Alamillo-Ferrer, [b] Jordi Bures, [b] Richard Procter, [c] Tom D. Sheppard [c] and Andrew Whiting [d]

Received 22nd May 2022,
Accepted 8th August 2022

DOI: 10.1039/d2cp02317b

rsc.li/pccp

We report the evaluation of density-functional-theory (DFT) based procedures for predicting ^{19}F NMR chemical shifts at modest computational cost for a range of molecules with fluorine bonds, to be used as a tool for assisting the characterisation of reaction intermediates and products and as an aid to identifying mechanistic pathways. The results for a balanced learning set of molecules were then checked using two further testing sets, resulting in the recommendation of the ωB97XD/aug-cc-pvdz DFT method and basis set as having the best combination of accuracy and computational time, with a RMS error of 3.57 ppm. Cationic molecules calculated without counter-anion showed normal errors, whilst anionic molecules showed somewhat larger errors. The method was applied to the prediction of the conformationally averaged ^{19}F chemical shifts of 2,2,3,3,4,4,5,5-octafluoropentan-1-ol, in which gauche stereoelectronic effects involving fluorine dominate and to determining the position of coordination equilibria of fluorinated boranes as an aid to verifying the relative energies of intermediate species involved in catalytic amidation reactions involving boron catalysts.

1 Introduction

Fluorinated molecules present a vast and important scope of uses, ranging from metallurgy (Hall–Héroult process) to pharmaceuticals.[1,2] For example organofluorines represent 10% of pharmaceuticals and up to 30% of agrochemicals.[3] Catalysis is one of the uses where the fluorine atom can shine, from helping stereospecificity to obtaining novel and more active catalysts.[3–7] As such it becomes important to have powerful and accurate tools in order to identify and characterize fluorinated compounds. Solution phase NMR spectroscopy has proven to be such a tool, especially with the introduction of standard continuous-flow adaptors for high-field instruments equipped with high-sensitivity multi-nuclear probes, which allows transient intermediates to be detected.[8–10] The need then is to augment such a tool with one that aids in structural assignments of the measured chemical shifts of all the detected species, including the transients. In addition, new methods have proven to be efficient for the synthesis of molecules using biologically active compounds, such as enzymes engineered to be specific for fluorinated substrates.[11] Such an NMR tool would prove useful for the rationalization, verification and improvement of these new strategies.

The increasing use of computational modelling based on DFT (density functional) methods (*in silico* chemistry) for probing catalytic mechanisms and structure is helping to change the approach to the design of new catalysts and such modelling can also play a role in helping to characterise intermediates and products using NMR methods.[12–15] An example of such application was the development of a computationally relatively cheap tool for ^{11}B NMR prediction for use in catalytic systems containing boron.[16] Previous studies of methods for predicting ^{19}F relative shifts have centred on small learning sets,[17–20] proteins[21,22] or based on collections of closely related molecules,[23–25] or even the influence of the solvation model.[26] Three studies stand out. Krivdin[18] presented a state-of-the-art review of the computational simulation of ^{19}F NMR. Many molecules are presented in various sets at various levels, but no "one for all" method was recommended, and many of the methods would be too computationally expensive for routine use with relatively large molecules (up to ~100 atoms). Fedorov[17] used two fluorinated molecules containing a total of 14 fluorine atoms for study, but such a model would require considerable extrapolation to the types of catalytic systems we

[a] *Department of Chemistry, Molecular Sciences Research Hub, Imperial College London, White City Campus, Wood Lane, London W12 OBZ, UK. E-mail: rzepa@imperial.ac.uk*
[b] *Department of Chemistry, The University of Manchester, Manchester M13 9PL, UK*
[c] *Department of Chemistry, Christopher Ingold Laboratories, University College London, 20 Gordon Street, London, WC1H 0AJ, UK*
[d] *Centre for Sustainable Chemical Processes, Department of Chemistry, Science Laboratories, Durham University, South Road, Durham, DH1 3LE, UK*

are interested in. The most recent from Benassi is a more complete study, albeit one in which the learning set differs greatly from the testing set and the resulting error is too large (>14 ppm) for the purpose of organofluorine and fluoroboron predictions.[27]

The present study is an extension to our previous method used for ^{11}B NMR.[16] Here we aim to benchmark a selection of methods based on combinations of DFT and other Hamiltonians and basis-sets that could help assignment of ^{19}F chemical shifts, using a carefully selected learning set of compounds appropriate for the study of catalysed reactions and their mechanisms utilizing fluorine as one analytic probe.

2 Computational and experimental details

Starting from the Organic Chemistry Database we identified 29 molecules with 88 unique chemical shifts as recorded in a variety of solvents.[28] This was reduced to 83 chemical shifts using Reaxys to corroborate the solvents/experimental conditions of the spectral measurements (see footnotes for excluded values).[29] During the selection procedure for what we refer to as the learning set, we noted that even for a simple compound such as $PhCF_3$, significant discrepancies in literature ^{19}F NMR chemical shifts can be observed. These have recently been comprehensively analysed and can be up to $\Delta\delta \pm 2.5$ ppm, albeit more typically $\Delta\delta \pm 1$ ppm, whilst identical samples run at different institutions still had an error of $\Delta\delta \pm 0.5$ ppm.[10] These statistics should be borne in mind when analysing the performance of any predictive method.

All the calculations presented here were performed using Gaussian 16, revision C.01. The CHAMP portal was used as an electronic notebook for managing the project, enabled with one-click FAIR data publishing to the Imperial College data repository.[30,31] All the solvents were modelled at the PCM level using the CPCM implementation.[32–34] The density functionals and Hamiltonians that were chosen for evaluation are: B3LYP,[35,36] ωB97XD[21] and MP2.[37–41] The basis sets were: aug-cc-pvdz,[42] Def2-svpp[43,44] and aug-pcSseq1.[45–48] In the case of the B3LYP calculations, the GD3+BJ[49] dispersion correction was included for geometry optimisation; the other two methods allow for dispersion either by similar correction or implicitly. NMR shieldings were computed using the Gauge-Independent Atomic Orbital (GIAO) method.[50–53] By default, an ultrafine DFT integration grid (99 590) was used, but a superfine grid (175 974, 2nd row atoms) along with high integral accuracy (10^{-14} a.u.) was also evaluated. This changed calculated shieldings by <0.04 ppm and fractional Boltzmann populations by <0.017. In the case of MP2 calculations, 2 magnetic tensors can be calculated: the MP2 GIAO method and the SCF GIAO one. Since the SCF GIAO RMSD was bigger than the MP2 one (7.93 ppm *versus* 5.59 ppm) and its R^2 was low (0.982), we discarded this method and only used the MP2 GIAO tensor for the following, under the name MP2/aug-cc-pvdz.

To predict the chemical shifts the following procedure was followed:

- Full optimisation and NMR calculation for the reference ($CFCl_3$) at each level and in each solvent.
- Full optimisation and NMR calculation for the molecule in the relevant solvents and at each level.
- Comparison for each calculated shift relative to the reference at the same level in the same solvent.

In order to determine the Boltzmann averaged chemical shifts for a species with multiple conformations such as 2,2,3,3,4,4,5,5-octafluoropentan-1-ol, the populations of the possible rotamers were calculated using the formula $\frac{N_i}{N_j} = e^{\frac{-\Delta_r G}{RT}}$ with $\Delta_r G$ being the difference of the Gibbs Free energies between the states, R the perfect gas constant and T the temperature (298.15 K in our case). These populations were used to weight the ^{19}F NMR shift for the fluorine atoms. All mathematical treatment was performed using python.

Since according to Roseneau *et al.*[10] the experimental error on the chemical shifts can be typically $\Delta\delta \pm 1.0$ ppm and up to 2.5 ppm, whereas the root mean square error on our calculated values (*i.e.* $\sqrt{\frac{\sum_{i=1}^{N}(\delta_{exp}-\delta_{calc})^2}{N}}$, with N being the number of chemical shifts) can range from 4 ppm to 16 ppm, we chose to perform our regression analysis on the calculated peaks in order to minimize the biggest error and to reveal any systematic errors in the calculated values. The regression analysis equation is therefore:

$$\delta_{calc} = \text{slope} \times \delta_{experimental} + \text{intercept} \quad (1)$$

According to Klaup *et al.*,[54] relativistic-based spin–orbit coupling corrections to the calculated shieldings of ^{19}F will be insignificant (<1 ppm), a correction similar to measurable chemical shift accuracy. Accordingly such corrections are not applied here, and they would in any case require specialised codes which would in itself defeat the purpose of this study in proposing a cheap and reliable tool for ^{19}F NMR chemical shift attribution.

2.1 Experimental details

Preparation of the pyridine adduct of difluoro(phenyl)borane: potassium phenyltrifluoroborate (18.4 mg, 0.1 mmol) was suspended in a mixture of anhydrous pyridine (450 μl) and pyridine-d5 (50 μl, with 0.3% v/v TMS) in a J Youngs NMR tube under an atmosphere of argon. Chlorotrimethylsilane (15.3 μl, 1.2 mmol) was added and the tube was sealed. The solid was dissolved by brief sonication and a fine white precipitate of KCl was observed. The sample was analysed by ^{11}B and ^{19}F NMR spectroscopy, using the tetramethylsilane peak as an internal reference. ^{11}B NMR (128 MHz, pyridine) δ = 6.24 ppm (br t). ^{19}F{^{1}H} NMR (376 MHz, pyridine) δ −154.6 (br s, 2H, PhBF2·Py); −156.3 ppm (s, 1H, ^{29}Si satellite J_{Si-F} = 275 Hz, TMSF).

2.2 Data availability

All the computational input and output files and experimental NMR primary datasets can be found as a FAIR data repository collection[55] and in associated sub-collections.

3 Results and discussion

3.1 Entries list and calculated chemical shifts

The list of solvents that were used as well as their calculated reference shielding constant can be found in the data repository collections.[55] The list of the molecules we selected, their solvent, as well as their experimental chemical shifts can be found in Table 1:

Excluding entries 27, 29, 70, 73 and 85 for reasons noted in the footnotes, there are a total of 83 entries for the learning set. The calculated values will be sorted by the method (Hamiltonian) used to calculate the wavefunction. This set of molecules will be called the Learning Set (LS) in the discussion. The results for the ωB97xd, MP2 and B3LYP methods can be found in Tables 2, 3 and 4 respectively.

Considering that species such as CF_3COOH are known for forming stable H-bonded dimers at higher concentrations, we investigated how large the effect on the predicted chemical shift of such self-aggregation or aggregation with explicit solvent molecules would be at the ωB97xd/aug-cc-pvdz level. The results can be found in Table 5:

The difference between the computed ^{19}F shift for CF_3COOH monomer and the various aggregated forms is always less than 1.1 ppm, which is within both experimental and computational error. Furthermore, the relatively low concentrations of substrate used for most NMR measurements would not favour self-aggregations.

A Bland–Altman plot at the ωB97xd/aug-cc-pvdz level for our learning set in Fig. 1 shows more than 95% of the values are contained within the interval mean $\pm 2\sigma$ and no obvious linear correlation appears.[118] From this, we conclude that the learning Set is well-behaved for our study.

Table 1 Selected molecules, their solvent, experimental chemical shifts (ppm) and entry value

Entry	Molecule	Solvent	δ_{exp}(ppm)
1	$CFCl_3$	N/A	Ref
2	CF_4	Acetone	-64.4[57]
3	hexafluorobenzene	Benzene	-162.9[58]
4		THF	-165[60]
5		Acetonitrile	-165.2[62]
6		MeOH	-162.554[59]
7		DMSO	-162.5[64]
8	CF_3Cl	DCM	-27.96[66]
9	$FCH_2C{\equiv}N$	Chloroform	-231.9[68]
10	$CFCl_2-CFCl_2$	DCM	-72.06[66]
11		Chloroform	-68.6[71]
12	α,α,α-trifluorotoluene	Chloroform	-63.72[73]
13		DCM	-63.3[75]
14		Acetonitrile	-63.3[77]
15		o-DCB	-63[79]
16		DMF	-61.384[81]
17		THF	-62.6[83]
18	CF_3H	Acetone	-79[85]
19		DMSO	-77.35[87]
20		Acetonitrile	-79.87[88]
21		MeOH	-80[90]
22		Toluene	-79.475[92]
23		THF	-79.17[92]
24		Benzene	-79[93]
25		DCM	-78.33[66]
26	difluoro(phenyl)borane	hexane	-92.89[95]
27		THF[a]	-142[97]
28		Chloroform	-92[98]
29		Acetonitrile[a]	-127.9[98]
30	2,2,2-trifluoroacetyl fluoride	Acetone	16.7[101]
31			-74.9[101]
32		DCM	16.4[104]
33			-74.5[104]
34	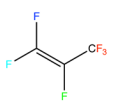	Benzene	-72[107]
35			-91[107]
36			-105[107]
37			-195[107]
38		Diethylether	-70.9[111]
39			-91.6[111]
40			-106.1[111]
41			-195.7[111]
42		Acetone	-69[101]
43			-91.75[101]
44			-105.8[101]
45			-192.9[101]
46	CF_3COOH	DCM	-75[56]
47		Acetone	-75.5[57]
48		MeOH	-74.742[59]
49		H_2O	-77.7[61]
50	$BF_3\cdot THF$	Chloroform	-155.33[4]
51	fluorobenzene	Benzene	-112.8[63]
52		Acetonitrile	-114.9[65]
53		THF	-113.15[67]
54		Chloroform	-113.066[69]
55		DCM	-114.29[70]
56		DMSO	-113.6[72]
57		Cyclohexane	-113.4[74]
58		H_2O	-112.97[76]
59		CCl_4	-112.9[78]
60	$(CF_3)_2C{=}O$	DCM	-82.9[80]
61	allyldifluoroborane	Chloroform	-73.2[82]
62	1,4-difluorobenzene	Acetonitrile	-120.73[84]
63		heptane	-120[86]
64		THF	-121[3]
65		DMF	-120.01[89]
66		Acetone	-121.6[91]
67		Chloroform	-120.05[78]
68		CCl_4	-119.67[78]
69		hexane	-120.1[78]
70	BF_3[b]	DCM	-153.2[94]
71	1,1,1-trifluoroethane	THF	-60[96]
72		DCM	-61.3[66]
73	CH_3OF[c]	Acetonitrile	120.3[99]
74	2-fluoro-2-methylpropane	DCM	-134.3[100]
75	Octafluorocyclobutane	Chloroform	-134[102]
76	1,2-difluoroethyne	Toluene	-261.3[103]
77	$CF_3C{\equiv}CCF_3$	Chloroform	-53.5[105]
78	(E)-1-fluoroprop-1-ene	Acetone	-129.5[106]
79	(Z)-1-fluoroprop-1-ene	Acetone	-131[106]
80	3-fluoroprop-1-ene	Chloroform	-216.2[108]
81	fluoromethane	Acetone	-261.9[109]
82		Benzene	-267.6[110]
83		DMSO	-272.4[112]
84		Chloroform	-266.5[113]
85		Cyclohexane[a]	-205[114]
86	fluoroethane	o-DCB	-209.9[115]
87		Diethylether	-212[116]
88		Chloroform	-212.4[117]

[a] Three different values in different solvents are observed. We discuss this further in Section 4.2. [b] BF_3 is reported as a reaction product, but its coordination to this solvent is unknown. [c] Molecules containing O–F or N–F bonds are considered to be very highly correlated species of a type that DFT theory using small basis sets cannot adequately represent and are not included in the analysis here. For further discussion, see Section 3.3.1.

Table 2 Calculated chemical shifts of the learning set at the ωB97xd/aug-cc-pvdz, ωB97xd/aug-pcSseq1 and ωB97xd/Def2-svpp levels. All the values are in ppm

Entry	$\delta_{\omega b97xd/}$ aug-pvdz	$\delta_{\omega b97xd/}$ pcSseq1	$\delta_{\omega 97xd/}$ def2svpp	Entry	$\delta_{\omega b97xd/}$ aug-pvdz	$\delta_{\omega b97xd/}$ pcSseq1	$\delta_{\omega b97xd/}$ def2svpp
1	0.00	0.00	0.00	46	−77.46	−83.82	−66.87
2	−61.35	−65.31	−50.90	47	−77.32	−83.80	−66.90
3	−158.56	−174.56	−146.23	48	−77.26	−83.79	−66.93
4	−159.07	−175.10	−146.68	49	−77.25	−83.78	−66.92
5	−159.11	−175.19	−146.85	50	−160.49	−170.99	−134.91
6	−159.20	−175.44	−146.81	51	−116.09	−122.17	−92.63
7	−159.11	−175.35	−146.86	52	−117.72	−123.96	−93.95
8	−29.10	−30.33	−20.04	53	−117.45	−123.51	−93.57
9	−235.51	−254.25	−228.71	54	−117.08	−123.11	−93.31
10	−66.53	−70.50	−61.98	55	−117.55	−123.56	−93.82
11	−66.70	−70.52	−62.12	56	−117.74	−124.14	−93.98
12	−64.89	−70.01	−55.25	57	−115.89	−121.99	−92.46
13	−65.33	−69.77	−54.99	58	−117.77	−124.19	−94.01
14	−65.20	−69.55	−54.95	59	−116.06	−122.22	−92.61
15	−65.30	−69.73	−55.04	60	−81.83	−83.38	−66.42
16	−65.20	−69.56	−54.95	61	−75.53	−80.46	−47.78
17	−65.36	−69.82	−55.13	62	−123.66	−130.10	−100.21
18	−81.54	−87.13	−69.49	63	−122.44	−128.88	−99.20
19	−81.50	−87.13	−69.54	64	−123.49	−129.92	−99.97
20	−81.53	−87.13	−69.53	65	−123.66	−130.09	−100.21
21	−81.54	−87.13	−69.52	66	−123.63	−130.12	−100.14
22	−81.99	−87.04	−69.23	67	−123.37	−129.66	−99.80
23	−81.67	−87.11	−69.44	68	−122.62	−129.06	−99.37
24	−81.61	−87.03	−69.21	69	−122.42	−128.86	−99.18
25	−81.61	−87.12	−69.36	71	−65.27	−70.58	−57.81
26	−95.87	−101.36	−69.15	72	−65.15	−70.53	−57.68
28	−96.82	−102.18	−69.72	74	−146.81	−155.30	−148.01
30	18.76	18.89	36.33	75	−133.97	−146.36	−124.36
31	−76.55	−82.98	−66.72	76	−263.97	−286.50	−250.06
32	−76.70	−83.06	−66.71	77	−55.36	−60.27	−47.19
33	18.58	18.77	36.31	78	−132.05	−140.23	−101.56
34	−71.53	−76.86	−60.58	79	−135.77	−143.36	−105.15
35	−87.83	−94.53	−72.10	80	−213.11	−229.56	−206.80
36	−102.40	−107.41	−83.67	81	−272.60	−292.94	−248.15
37	−191.54	−203.31	−176.87	82	−272.19	−292.46	-247.31
38	−71.43	−76.68	−60.35	83	−272.60	−292.98	−248.25
39	−87.38	−93.90	−71.49	84	−272.60	−292.76	−247.79
40	−101.97	−106.79	−83.05	86	−219.44	−235.40	−207.20
41	−192.23	−203.87	−177.46	87	−219.43	−235.24	−206.96
42	−55.83	−76.38	−60.11	88	−219.43	−235.27	−207.00
43	−86.52	−93.24	−70.86				
44	−101.14	−106.15	−82.41				
45	−192.54	−204.45	−178.04				

Table 3 Calculated chemical shifts of the learning set at the MP2/aug-cc-pvdz level (ppm)

Entry	MP2/aug-cc-pvdz	Entry	MP2/aug-cc-pvdz	Entry	MP2/aug-cc-pvdz	Entry	MP2/aug-cc-pvdz
1	0.00	22	−81.48	45	−199.97	66	−127.82
2	−64.13	23	−81.49	46	−77.86	67	−127.36
3	−166.29	24	−81.25	47	−77.79	68	−126.73
4	−166.98	25	−81.46	48	−77.50	69	−126.44
5	−167.12	26	−70.66	49	−77.72	71	−65.51
6	−166.87	28	−71.97	50	−160.86	72	−65.42
7	−167.13	30	1.25	51	−120.87	74	−142.98
8	−31.25	31	−77.74	52	−122.43	75	−136.38
9	−230.67	32	−74.90	53	−122.08	76	−271.01
10	−67.66	33	16.70	54	−121.71	77	−55.62
11	−67.66	34	−72.19	55	−122.17	78	−139.05
12	−64.53	35	−97.31	56	−122.45	79	−143.41
13	−63.39	36	−110.78	57	−120.65	80	−207.91
14	−64.11	37	−199.05	58	−122.48	81	−270.47
15	−64.36	38	−52.00	59	−120.89	82	−270.07
16	−64.11	39	−96.92	60	−78.28	83	−270.46
17	−64.43	40	−111.40	61	−82.03	84	−270.29
18	−81.46	41	−199.48	62	−127.85	86	−215.99
19	−81.41	42	−71.87	63	−126.47	87	−215.72
20	−81.44	43	−96.56	64	−127.64	88	−215.78
21	−81.18	44	−111.06	65	−127.85		

3.2 Regression analysis

The evaluation of two different DFT functionals applied with various basis sets as well as MP2 method was based on 83 ^{19}F NMR peaks, covering a wide range of chemical shifts (−260 ppm to −20 ppm). The regression analysis using eqn (1) obtained by least squares minimisation of the calculated chemical shifts can be found in Table 6. The provided root mean square deviations (RMSD) were obtained using the following equation:

$$\mathrm{RMSD} = \sqrt{\frac{\sum_{i=1}^{N}\left(\delta_{\mathrm{calc}} - \left(\mathrm{slope} \times \delta_{\mathrm{exp}} + \mathrm{intercept}\right)\right)^2}{N}} \qquad (2)$$

with N being the number of experimental chemical shifts (*e.g.* ref. 83).

The ωB97xd/aug-cc-pvdz method shows low RMSD values (Table 6) and an intercept close to zero. The largest RMSD corresponds to 2.64% of the total chemical shift range, while the lowest is 1.24% over the same range. Over this range, the slope tends to be s

The computational cost of the various methods does not correlate well with their accuracy. Thus although the method with the highest R^2, ωB97xd/aug-pcSseq1 also has a small RMSD (3.64 ppm), it is approximately 24 times slower to complete than at the ωB97xd/Def2-svpp level. B3LYP/aug-cc-pvdz displays the same features, a good R^2, somewhat larger RMSD but clearly non-zero intercepts. The relatively expensive MP2/aug-cc-pvdz combination is not superior to the ωB97xd/aug-cc-pvdz method, but might prove more reliable for molecules with correlated or unusual bonds.

For this type of calculations, based on the parameters, R^2, RMSD, slope, intercept and the standard errors, we recommend the ωB97xd/aug-cc-pvdz level, which also has the advantage of being affordable in terms of CPU resources. This is in line with our previous report on ^{11}B NMR[16] and gives the advantage that both the ^{19}F and ^{11}B nuclei can be computed at the same level in a single calculation for molecules containing both elements. The regression coefficients (slope ∼ unity, intercept ∼ 0) means the unadjusted calculated value could be used to assign experimental shifts with an average mean error of 3.9 ppm.

$$\delta_{\mathrm{calc}} \approx \delta_{\mathrm{exp}} \qquad (3)$$

Rearranging eqn (1) allows correction for the systematic errors; in eqn (4) δ_{pred} indicates the predicted chemical shift.

$$\delta_{\mathrm{pred}} = \frac{\delta_{\mathrm{calc}} + 0.02534}{1.0112} \qquad (4)$$

Table 4 Calculated chemical shifts of the learning set at the B3LYP/Def2svpp, B3LYP/aug-cc-pvdz, B3LYP+GD3-BJ/aug-cc-pvdz and B3LYP+GD3-BJ/Def2svpp levels (ppm)

Entry	B3LYP/ Def2svpp	B3LYP/ aug-cc-pvdz	B3LYP+GD3-BJ/ augc-cc-pvdz	B3LYP+GD3-BJ/ Def2svpp
1	0.00	0.00	0.00	0.00
2	−59.10	−71.67	−71.14	−58.59
3	−154.08	−168.98	−168.64	−153.77
4	−154.60	−169.53	−169.20	−154.30
5	−154.78	−169.75	−169.41	−154.49
6	−154.76	−169.47	−169.22	−154.46
7	−154.79	−169.76	−169.41	−154.50
8	−26.48	−37.02	−36.54	−26.04
9	−237.78	−245.51	−245.04	−237.10
10	−64.60	−69.49	−70.19	−65.37
11	−64.62	−69.70	−70.41	−65.00
12	−63.46	−74.68	−74.32	−62.81
13	−63.29	−74.38	−74.01	−63.05
14	−63.14	−74.19	−73.84	−62.80
15	−63.26	−74.39	−74.03	−62.91
16	−63.13	−74.19	−73.83	−62.80
17	−63.32	−74.48	−74.12	−62.98
18	−75.57	−90.44	−89.90	−75.03
19	−75.60	−90.45	−89.90	−75.08
20	−75.58	−90.44	−89.90	−75.88
21	−75.59	−90.44	−89.90	−75.05
22	−75.17	−90.44	−89.89	−74.65
23	−75.48	−90.45	−89.91	−74.94
24	−75.13	−90.43	−89.89	−74.63
25	−75.58	−−90.45	−89.91	−75.06
26	−78.61	−110.99	−110.68	−78.30
28	−79.24	−111.98	−111.64	−78.67
30	31.52	10.84	11.18	31.84
31	−74.02	−85.28	−84.89	−73.62
32	−74.11	−85.41	−85.03	−73.83
33	31.43	10.71	11.05	31.63
34	−68.21	−80.55	−80.19	−67.12
35	−79.37	−97.20	−96.85	−78.29
36	−90.36	−111.36	−110.95	−89.29
37	−183.10	−199.70	−199.39	−182.05
38	−67.97	−80.21	−79.86	−67.61
39	−78.78	−96.55	−96.19	−78.45
40	−89.79	−110.71	−110.34	−89.43
41	−183.71	−200.21	−199.90	−183.37
42	−67.76	−79.91	−79.55	−67.38
43	−78.18	−95.87	−95.52	−77.82
44	−89.20	−110.07	−109.70	−88.85
45	−184.33	−200.73	−200.42	−183.99
46	−74.23	−86.29	−85.92	−73.93
47	−74.20	−86.24	−85.87	−73.84
48	−74.20	−86.23	−85.86	−73.82
49	−74.18	−86.36	−85.99	−73.82
50	−146.87	−177.82	−176.29	−146.54
51	−98.54	−126.18	−125.79	−98.17
52	−100.04	−128.21	−127.81	−99.66
53	−99.62	−127.64	−127.24	−99.24
54	−99.33	−127.24	−126.84	−98.65
55	−99.70	−127.75	−127.36	−99.34
56	−100.06	−128.24	−127.84	−99.69
57	−98.36	−125.95	−125.55	−97.85
58	−100.10	−128.31	−127.89	−99.72
59	−97.51	−126.15	−125.75	−98.14
60	−74.08	−86.64	−86.31	−73.84
61	−55.32	−88.60	−87.99	−54.47
62	−106.37	−133.90	−133.51	−105.97
63	−105.03	−132.35	−131.97	−104.67
64	−106.10	−133.53	−133.16	−105.73
65	−106.34	−133.90	−133.51	−106.00
66	−106.32	−133.83	−133.43	−105.95
67	−105.88	−133.29	−132.91	−105.19
68	−104.20	−132.57	−132.18	−104.82
69	−105.01	−132.34	−131.95	−104.64
71	−66.53	−74.82	−74.40	−66.14
72	−66.59	−74.74	−74.33	−66.12
74	−154.91	−154.82	−154.94	−155.13
75	−133.18	−142.96	−143.00	−132.58
76	−263.09	−280.50	−279.98	−262.59
77	−53.20	−62.46	−62.01	−52.46
78	−107.76	−142.91	−142.50	−107.37
79	−111.93	−146.34	−145.93	−142.54
80	−213.52	−220.81	−220.18	−212.67
81	−257.91	−286.70	−286.15	−257.38
82	−256.86	−286.28	−285.72	−256.33
83	−257.99	−286.73	−286.18	−257.46
84	−257.47	−286.52	−285.96	−256.63
86	−213.59	−229.22	−228.62	−213.02
87	−213.23	−229.01	−228.42	−212.66
88	−213.29	−229.04	−228.45	−212.42

Table 5 Comparison between the experimental ^{19}F chemical shifts and the computed values of different aggregation models of CF_3COOH

System	Solvent	Chemical shift (ppm)	Error (ppm)
Exp.	Acetone	−75.5[57]	
Monomer		−77.32	1.82
Dimer		−78.19	2.69
H-Bond donor 1		−78.39	2.89
H-Bond donor 2		−77.28	1.78
Exp.	DCM	−75[56]	
Monomer		−77.46	2.46
Dimer		−78.33	3.33
Exp.	H_2O	−77.7[61]	
Monomer		−77.25	0.45
Dimer		−78.11	0.41
H-Bond donor 1		−78.27	0.57
H-Bond donor 2		−76.707	1.00
H-Bond acceptor 1		−77.11	0.59
H-Bond acceptor 2		−77.08	0.62
H-Bond acceptor 3		−76.57	1.13
H-Bond acceptor 4		−76.41	1.29
Exp.	MeOH	−74.742[59]	
Monomer		−77.26	2.52
Dimer		−78.15	3.41
H-Bond donor 1		−78.35	3.60
H-Bond donor 2		−77.13	2.39
H-Bond acceptor 1		−77.29	2.55
H-Bond acceptor 2		−77.10	2.36
H-Bond acceptor 3		−76.67	1.93
H-Bond acceptor 4		−76.44	1.70

In that case the error is on average expected to be 3.53 ppm. This error was calculated using:

$$\mathrm{RMSD} = \sqrt{\frac{\sum_{i=1}^{N}\left(\delta_{\mathrm{exp}} - \left(\frac{\delta_{\mathrm{calc}} + 0.2534}{1.0112}\right)\right)^2}{83}} \quad (5)$$

Fig. 2 shows the regression plot at the ωb97xd/aug-cc-pvdz level using eqn (3). The other regression plots can be found in the repository data collection.[119]

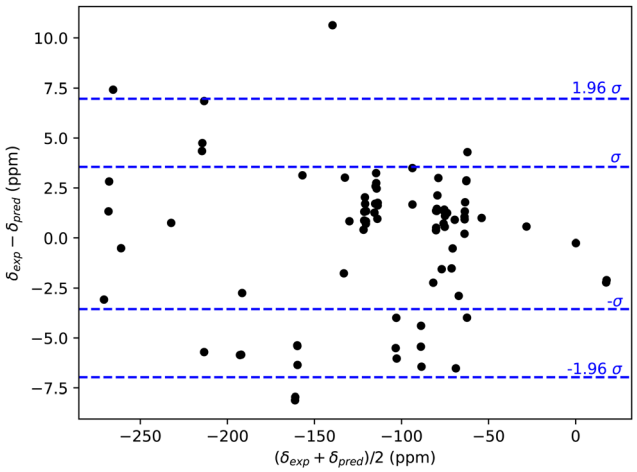

Fig. 1 Bland–Altman plot[118] for the learning set.

Table 6 Regression analysis for the learning set ^{19}F NMR chemical shifts using eqn (1)

	Slope with std error σ	Intercept with std error σ (ppm)	R^2	RMSD (ppm)
ωB97xd/aug-cc-pvdz	1.01 ± 0.01	−0.25 ± 0.82	0.9968	3.57
ωB97xd/aug-pcSseq1	1.09 ± 0.01	0.66 ± 0.85	0.9971	3.64
ωB97xd/Def2-svpp	0.98 ± 0.01	11.95 ± 1.68	0.9861	7.23
MP2/aug-cc-pvdz	1.00 ± 0.01	−3.56 ± 1.29	0.9921	5.53
B3LYP/Def2-svpp	0.99 ± 0.01	6.37 ± 1.73	0.9856	7.45
B3LYP/aug-cc-pvdz	1.03 ± 0.01	−7.52 ± 1.08	0.9948	4.66
B3LYP+GD3BJ/aug-cc-pvdz	1.03 ± 0.01	−7.24 ± 1.06	0.9950	4.55
B3LYP+GD3BJ/Def2-svpp	0.99 ± 0.01	6.45 ± 1.78	0.9849	7.63
ωB97xd/aug-cc-pvdz[a]	0.96 ± 0.00	−6.34 ± 0.40	0.9966	2.31

[a] This linear regression is for testing set 2 (see Section 3.3.2 for more detail).

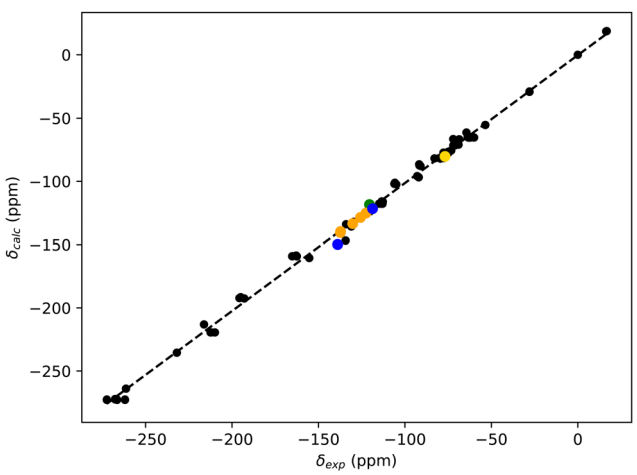

Fig. 2 Regression plot at the ωB97xd/aug-cc-pvdz level. The dashed line correspond to the linear regression. The blue dots correspond to the trifluoro(4-fluorophenyl)borate, the orange dots correspond to the 2-2-3-3-4-4-5-5-octafluoropentan-1-ol, the golden dot corresponds to tris(2-2-2-trifluoroethyl) borate and the green dot to 1-fluoro-2-nitrobenzene.

3.3 Testing sets and identification of sources of error

3.3.1 Testing set 1. We tested both least-squares eqn (3) and (4) on four different molecules expressing nine different chemical shifts. These 4 molecules (and ^{19}F NMR values) were suggested by our collaborators as part of our current catalytic study. This set of molecules is referred to as Testing Set 1. The calculated chemical shifts can be found in Table 7 and the absolute errors in Table 8.

The outlier in this set is the −138.9 ppm measured value for trifluoro(4-fluorophenyl)borate as assigned to the negatively charged trifluoroborate unit. The predicted values show large variation using the computational methods, the errors ranging from 2.60 ppm (B3LYP+GD3BJ/Def2-svpp) to 30.90 ppm (B3LYP/aug-cc-pvdz) using eqn (3), and 6.21 ppm (ωB97xd/Def2-svpp) to 18.37 ppm (B3LYP/aug-cc-pvdz) with eqn (4) (Table 8). To find out whether the effect is general to fluoroborate anions, we searched the CSD (Cambridge Structure Database) for other molecules containing this motif, to determine if any relationship between their predicted solution state ^{19}F chemical shifts and the closest approach of the counter-cation in the solid state might exist. Of the 31 matches, 10 were selected for analysis, having both reported ^{19}F chemical shift values in solution and available for calculation using the calibrated aug-cc-pvdz basis set. The experimental and calculated chemical shifts as well as the CSD reference code and absolute errors can be found in Table 9. For GABCEV[120] the values reported in the article for the ^{19}F and ^{11}B NMR (−63.5 ppm and 64.1 ppm respectively) do not match what should be expected experimentally (approximately −140 ppm for the ^{19}F and 5 ppm for the ^{11}B) or by calculation, but those reported in the article ESI do match and are shown in the table. The corresponding plot and structures can be found in Table 9 and Fig. 3 and 4 respectively.

Where the cationic component is present intramolecularly, the predicted errors can be no larger than the RMS error, but when omitted as intermolecular components, the errors can be as large as 11.4 ppm. Significantly, there is no relationship between the error and the closest approach of the counter-cation in the solid state. To probe further, we then returned to focus on trifluoro(4-fluorophenyl)borate itself by modelling the shift in solution with various forms of an alkali metal counter-ion present. Since K^+ is not defined at the aug-cc-pvdz basis set level, we replaced it with Na^+. The errors for the chemical shifts obtained *via* eqn (4) are provided in Table 10. The calculated structures for the various complexes of trifluoro(4-fluorophenyl)borate can be found in Fig. 5.

We first tested if inclusion of Na^+ alone improved the prediction compared to its absence at the ωB97xd/aug-cc-pvdz level, but the error was only modestly reduced. Next, we complexed the Na^+ ion to a DMSO (solvent) molecule. Reasonable agreement with experiment was only obtained with 6DMSO·Na^+, suggesting that not only the position but also the explicit solvation of the counter-cation for such fluoroborate anions may be important for more accurate ^{19}F NMR chemical shift predictions. However, such a model increases the size of the system and hence the computational cost significantly. Furthermore optimising the position of the solvated counter-ion can be non-trivial and so this

Table 7 Testing set 1 ^{19}NMR calculated chemical shifts (ppm)

Molecule	Solvent	Peak (ppm)	ωB97xd/aug-cc-pvdz	ωB97xd/Def2-svpp	ωB97xd/aug-pcSseq1	MP2/aug-cc-pvdz
1-Fluoro-2-nitrobenzene	Acetonitrile	−120.5	−118.37	−98.27	−125.23	−131.85
2,2,3,3,4,4,5,5-Octafluoropentan-1-ol	Chloroform	−122.5	−124.36	−109.32	−132.06	−124.26
		−125.7	−127.18	−112.57	−135.31	−126.25
		−130.2	−132.24	−117.22	−140.79	−132.53
		−137.2	−141.16	−126.95	−151.17	−140.63
		−137.3	−141.75	−127.37	−151.69	−141.24
Trifluoro(4-fluorophenyl)borate	DMSO	−118.7	−123.70	−101.98	−130.54	−126.23
		−138.9	−153.62	−130.32	−164.45	−151.40
Tris(2,2,2-trifluoroethyl)borate	Chloroform	−76.8	−80.30	−78.26	−86.42	−80.68

Molecule	Solvent	Peak (ppm)	B3LYP/ Def2-svpp	B3LYP/ aug-cc-pvdz	B3LYP+GD3BJ/ aug-cc-pvdz	B3LYP+GD3BJ/ Def2-svpp
1-Fluoro-2-nitrobenzene	Acetonitrile	−120.5	−103.11	−125.62	−125.37	−102.90
2,2,3,3,4,4,5,5-Octafluoropentan-1-ol	Chloroform	−122.5	−118.86	−130.40	−133.75	−117.95
		−125.7	−120.63	−137.42	−137.08	−120.93
		−130.2	−125.10	−142.06	−141.48	−124.87
		−137.2	−133.86	−150.76	−150.14	−133.42
		−137.3	−134.49	−151.37	−150.81	−133.96
Trifluoro(4-fluorophenyl)borate	DMSO	−118.7	−108.55	−134.17	−133.78	−108.19
		−138.9	−141.90	−169.80	−169.38	−141.50
Tris(2,2,2-trifluoroethyl)borate	Chloroform	−76.8	−78.49	−89.86	−89.61	−77.67

Table 8 Absolute errors and RMSD using eqn (4) applied to the ^{19}NMR chemical shifts (ppm) for testing set 1

Molecule	Solvent	Peak (ppm)	ωB97xd/aug-cc-pvdz	ωB97xd/Def2-svpp	ωB97xd/aug-pcSseq1	MP2/aug-cc-pvdz
1-Fluoro-2-nitrobenzene	Acetonitrile	−120.5	3.69	8.08	4.93	7.98
2,2,3,3,4,4,5,5-Octafluoropentan-1-ol	Chloroform	−122.5	0.22	1.17	0.67	1.97
		−125.7	0.18	1.31	0.87	3.15
		−130.2	0.33	1.55	0.34	1.38
		−137.2	2.14	4.47	2.19	0.30
		−137.3	2.63	4.80	2.57	0.22
Trifluoro(4-fluorophenyl)borate	DMSO	−118.7	3.37	2.50	1.75	4.22
		−138.9	12.77	6.21	12.68	8.92
Tris(2,2,2-trifluoroethyl)borate	Chloroform	−76.8	2.36	15.21	3.15	1.06
		RMSD	4.77	6.58	4.84	98.99

Molecule	Solvent	Peak (ppm)	B3LYP/ Def2-svpp	B3LYP/ aug-cc-pvdz	B3LYP+GD3BJ/ aug-cc-pvdz	B3LYP+GD3BJ/ Def2-svpp
1-Fluoro-2-nitrobenzene	Acetonitrile	−120.5	10.22	6.05	5.92	10.40
2,2,3,3,4,4,5,5-Octafluoropentan-1-ol	Chloroform	−122.5	3.63	3.44	0.19	2.74
		−125.7	2.24	0.18	0.24	2.55
		−130.2	2.23	0.17	0.01	2.02
		−137.2	4.06	1.60	1.40	3.63
		−137.3	4.59	2.10	1.95	4.07
Trifluoro(4-fluorophenyl)borate	DMSO	−118.7	2.94	4.03	4.04	3.28
		−138.9	10.46	18.35	18.37	10.07
Tris(2,2,2-trifluoroethyl)borate	Chloroform	−76.8	8.68	2.99	3.09	7.90
		RMSD	6.31	6.81	6.70	6.06

computational tool may no longer be necessarily considered a rapid one, which was one of our objectives in this study.

We concluded our examination of ionic species by investigating seven further solution-phase ionic compounds from Roseneau *et al.*[10] (entries 88, 90–92, 97, 100 and 111 as referenced in the Roseneau tabulation), in this case without including their counter-ions. The experimental chemical shifts, the calculated ^{19}F NMR chemical shifts and the absolute errors for the estimated shifts can be found in Table 11, while their structures can be found in Fig. 6.

We notice, as have others, that N–F bonds seem to be a significant source of errors, which is not surprising since these types of bonds are very electron rich and hence more highly correlated than *e.g.* C–F bonds. We do not report the values here but note that O–F bonds were also sources of large errors (sometimes >50 ppm, with a 400 ppm error on the F_2O_2), for the same reason. B–F bonds tend to occur on anionic components, which appear to have a slightly higher systematic error than neutral and cationic C–F systems (Table 11) and are discussed in more detail below.

Table 9 CCDC reference, experimental and chemical ^{19}F chemical shifts and counter-cation closest approach (Å)

Compound	Experimental	Calculated	Absolute error	Distance
CARKIR	−142[121]	−150.64	8.64	2.62
FUYDOT	−136.58[122]	−146.19	9.61	3.05
OZOJOD	−133.3[123]	−144.71	11.41	3.26
SEGMOJ	−138.6[124]	−140.67	2.07	2.81
SEGMUP	−135.6[124]	−141.53	5.93	2.86
SEGNAW	−137.6[124]	−144.51	6.91	2.97
YOWJIG	−143.33[125]	−153.99	10.66	2.82
ZUCWAY	−142.2[126]	−151.76	9.56	2.97
ZUCZOP	−143.5[126]	−154.12	10.62	2.68
GABCEV	−133.2[120]	−141.22	8.02	2.73

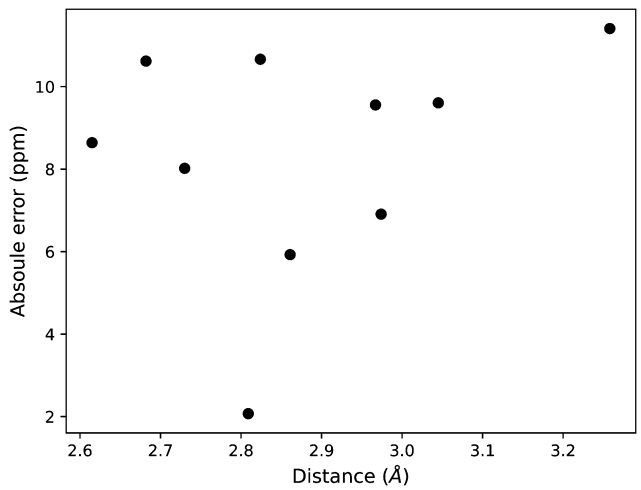

Fig. 3 Absolute error (ppm) as a function of the closest approach distance (Å) of the counter-cation for the fluoroborane motif as listed in in Table 9.

Anion 97 contains an Si–F bond for which two isomers were calculated, one with both fluorines axial and one axial and the other equatorial. The match to the experimental value for the diaxial isomer −104 ppm is better than the isomer. The error of 8.8 ppm for the diaxial isomer appears not to be due to the basis set lacking diffuse functions, as often used for anionic species (but ameliorated by the use of an anion-compactifying solvent field). Thus use of the d-aug-cc-pvdz basis (only available for first row elements) on F results in a predicted shift of −104.5 ppm, a slightly larger error than that observed without diffuse functions. A similar error was found for tetrafluoroborate anion itself (Table 9, entry 111) and the error is more probably due to lack of included counter-ion in the calculation as noted above. Cation 100 contains a C–F bond and is predicted well.

Table 10 ^{19}F NMR chemical shifts (ppm) and absolute errors evaluated using eqn (4) at the ωB97xd/aug-cc-pvdz level for the fluoroborate part of trifluoro(4-fluorophenyl)borate

Experimental	No Na^+	Na^+ complexed to F	Na^+ complexed to DMSO	Na^+ complexed to 6 DMSO
−138.9	−153.62	−151.39	−149.88	−142.23
Absolute error	12.77	10.56	9.07	3.33

Cation 92 also with a C–F bond was calculated as two rotameric orientations for the four isopropyl groups. Of these the conformation with the CH of the isopropyl being anti to the heterocyclic group had an error of 10.2 ppm and the other with the CH group *syn* was 1.0 ppm, which again shows that conformational analysis using this nucleus may be reliable. In general most cations are predicted accurately, which might suggest that the position and nature of the counter-anion may not be important, whereas anions may be more vulnerable to omission of a cationic counterion.

3.3.2 Testing set 2. Rosenau *et al.*[10] provide in their ESI (Table S6.2) a list of chemical shifts for 138 molecules. Eliminating the overlaps between this new set of molecules and our learning set (4), the molecules that have elements that lack basis set

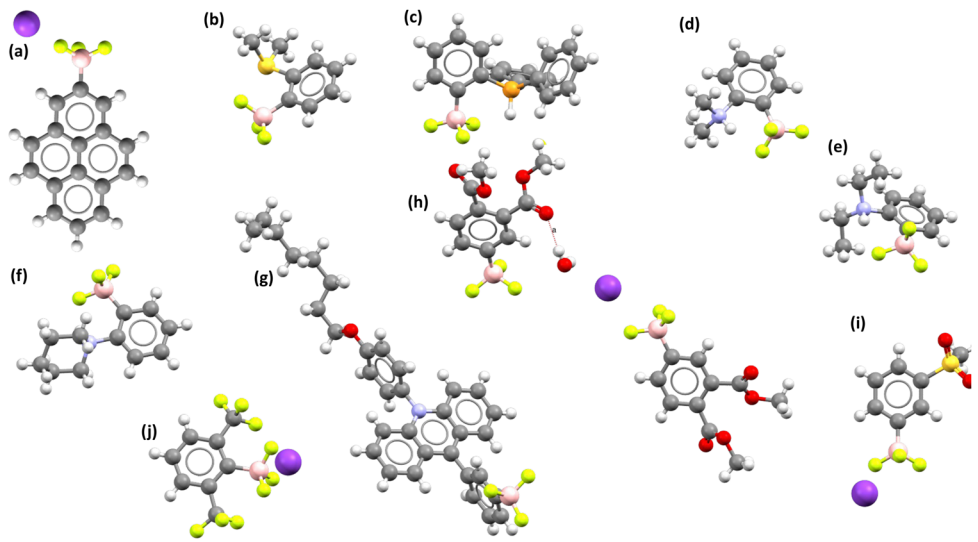

Fig. 4 Structures and Cambridge Refcode identifier of the trifluoro-(4-fluorophenyl)-borane like compounds. (a) CARKIR, (b) FUYDOT, (c) OZOJOD, (d) SEGMOJ, (e) SEGMUP, (f) SEGNAW, (g) YOWJIG, (h) ZUCWAY, (i) ZUCZOP and (j) GABCEV.

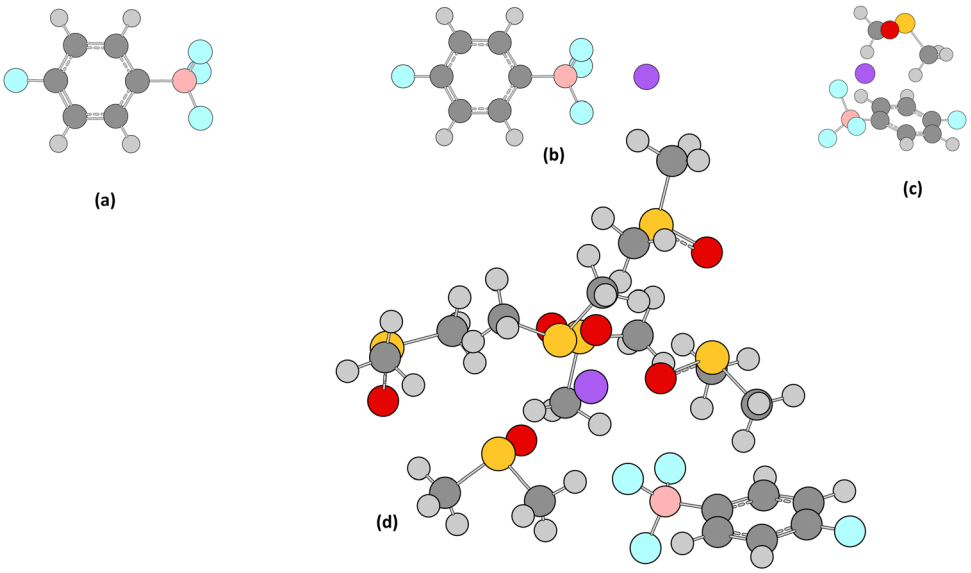

Fig. 5 Structures for trifluoro(4-fluorophenyl)borate complexed with Na^+ showing (a) no Na^+, (b) Na^+ complexed, (c) Na^+ complexed to DMSO and (d) Na^+ complexed to 6 DMSO.

Table 11 Experimental and calculated ^{19}F NMR chemical shifts (ppm) evaluated using eqn (4), with absolute errors of the estimated chemical shifts for entries 88, 90–92, 97, 100 and 111 selected from Roseneau *et al.*[10]

Entry	Experimental shift	Calculated shift	Absolute errors
88	48.16	18.05	30.11
90	16.03	−3.29	19.32
91	46.98	27.04	19.94
92	−107.51	−106.52	0.99
97, ax,eq	−95.20	−121.94	26.74
97, ax,ax	−95.20	−102.79	7.59
100	−53.11	−53.79	0.68
111	−152.84	−158.99	6.15

support, *e.g.* iodine (12) and these too far removed from the learning set such as hypercoordinate systems illustrated by 4-nitro(pentafluoro-sulfanyl)benzene (21), leaves 220 chemical shifts to be tested. We used these peaks as testing set 2, for both regression eqn (3) and (4) at the ωB97xd/aug-cc-pvdz level. Fig. 7 contain the plot of the predicted chemical shifts of these molecules as a function of the experimental ones. All the structures and chemical shifts can be found in the FAIR data repository collection.[127] Despite pushed to its limit, since many molecules in this new testing set are different from the learning set, such as these containing bromine or sulphur, we reach a RMSD of 3.16 ppm for eqn (4) with this new set over a range of 175 ppm, indicating the robustness of our prediction model. This RMSD was calculated using:

$$\mathrm{RMSD} = \sqrt{\frac{\sum_{i=1}^{N}\left(\delta_{\mathrm{exp}} - \left(\frac{\delta_{\mathrm{calc}} + 0.2534}{1.0112}\right)\right)^2}{220}} \qquad (6)$$

If we instead used this testing set as a learning set, obtaining a new a linear regression on these calculated peaks included in Table 6 and a lower RMSD (2.31 ppm). This further reduction in RMSD may also be also due to the very carefully calibrated set of chemical shift values used in this set, which emphasises the need to take especial care over referencing when making ^{19}F measurements. A Bland–Altman plot (Fig. 8) again shows that more than 95% of the values are contained within the interval mean $\pm 2\sigma$ and no obvious linear correlation appears.

4 Applications

4.1 Rotamers and stereoelectronic effects

A general problem in regard to predicting chemical shifts is for conformationally mobile systems. We evaluated one example of this, 2,2,3,3,4,4,5,5-octafluoropentan-1-ol in which stereoelectronic (*gauche* effect) alignments are possible. A search of the CSD (crystal structure database)[128] based on the substructure X–O–CH_2–CF_2–CFR–R′R″ (X = H, C) was conducted in two parts. The first search was for rotations about bonds 1 and 2 (Fig. 9) for examples that possessed both a primary alcohol or ether function and a fluorinated aliphatic side-chain and the second search for bonds 3 to 5 was for examples with fluorinated side-chains. This reveals a preponderance of *syn*-periplanar orientations ($\sim 60^\circ$) for vicinal heteroatom groups (Fig. 10).[129–139]

The five bonds about which three-fold rotations can occur in 2,2,3,3,4,4,5,5-octafluoropentan-1-ol results in $3^5 = 243$ possible rotamers. The crystal structure search (Fig. 9) suggests these could be dominated by gauche effects for all five rotational bonds. Approximate coordinates for these conformers were initially generated using the GMMX conformer dialogue in the Gaussview 6 program and then all were subjected to full energy minimisation and NMR calculation using the recommended ωB97xd/aug-cc-pvdz procedure. Applying eqn (4) leads to prediction errors that are only modestly larger than experimental

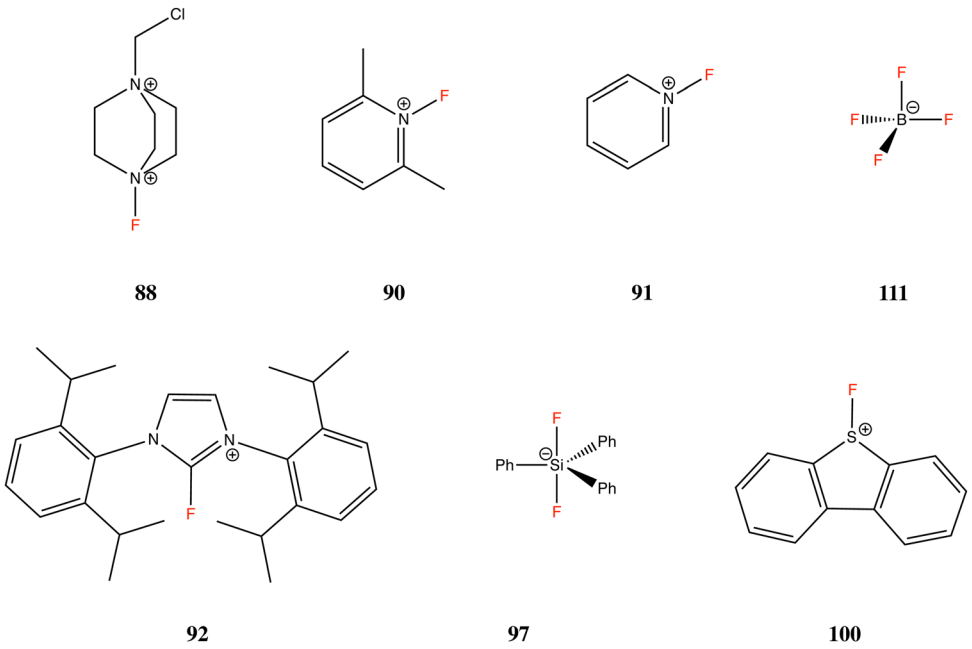

Fig. 6 Structures of the additional studied ions, with compounds numbered as in the ESI of Roseneau *et al.*[10]

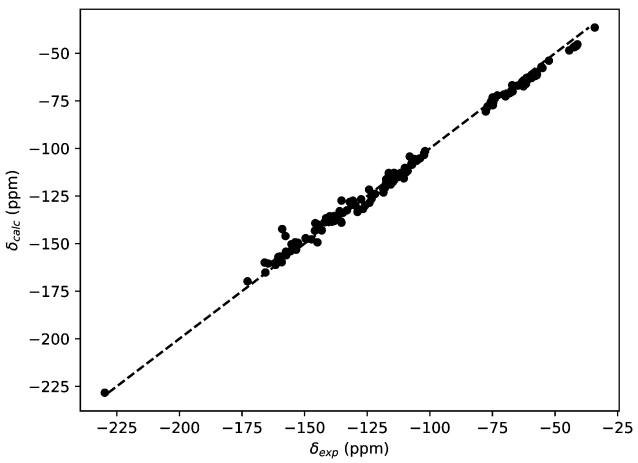

Fig. 7 ^{19}F NMR predicted chemical shifts for testing set 2 at the ωB97xd/aug-cc-pvdz level, eqn (3).

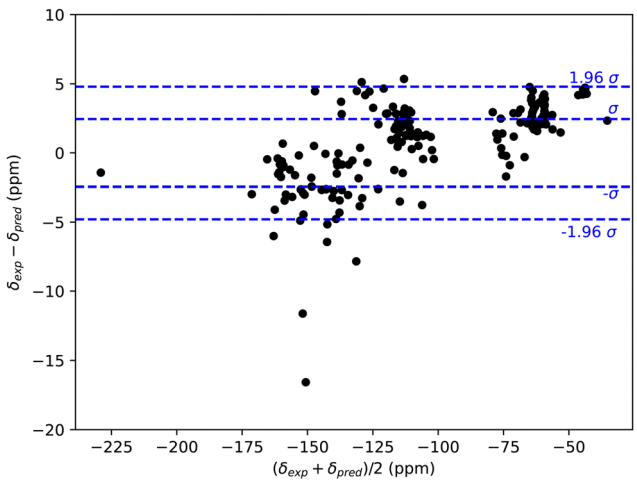

Fig. 8 Bland–Altman plot for testing set 2.

errors.[10] The global free energy minimum emerged as having nine gauche and several antiperiplanar orientations.

We compared 5 different sets: (i) those with all 225 non-duplicated rotamers, (ii) with the 20 (iii) 10 (iv) or 5 highest populated conformations and finally (v) the set with all 28 conformations having a population greater than 1%. The averaged chemical shifts and the populations can be found in the associated FAIR data repository, while the final corresponding RMSDs can be found in Table 12.[140] We note that these results are stable toward increasing the DFT quadrature to the more accurate superfine grid; 1.647 ppm for entry i, a potential source of error noted by Wheeler *et al.*[141]

This system is unusual in that selecting the 5 or 10 conformation subsets (iii) and (iv) produces a clearly inferior prediction and even selecting the set with populations >1% (set v) shows a significantly higher error than the full conformer set. In solution intermolecular hydrogen bonds and other effects can influence populations depending on the concentration of the NMR sample. These are not modelled here, but nonetheless the quality of the prediction using rotamer set i suggests that these may be less important than the desirability of including a full conformer space in the calculation.

4.2 Dissociative equilibria between 3- and 4-coordinate boron

The experimental values reported by Oisaki *et al.*[97] as well as Kim *et al.*[98] for difluoro(phenyl)borane (Table 1) in coordinating solvents do not align with these reported by Shmakov *et al.*[95] or Kim *et al.*[98] in non-coordinating chloroform. Tetrahyrofuran

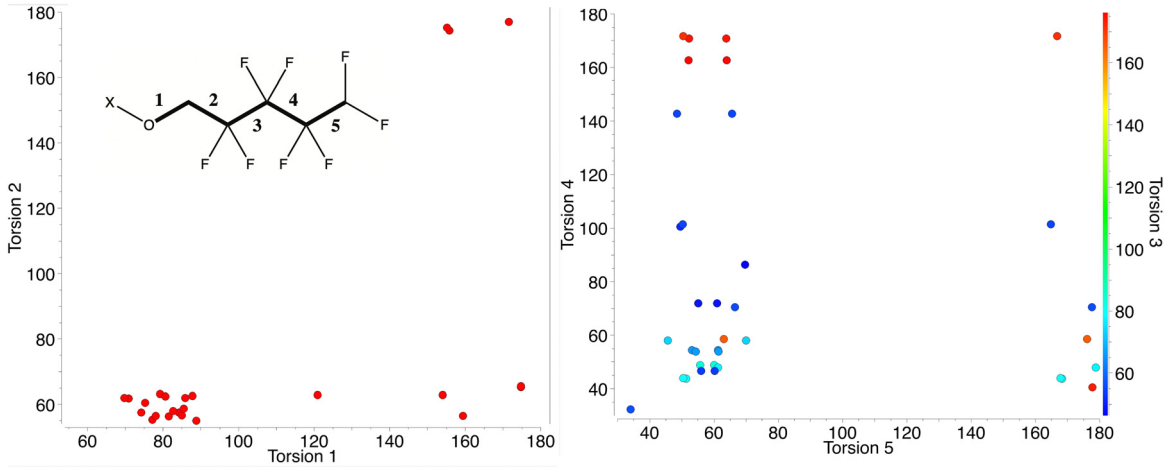

Fig. 9 A search of the CSD for molecules similar to 2,2,3,3,4,4,5,5-octafluoropentan-1-ol for values of bond torsions 1-5.

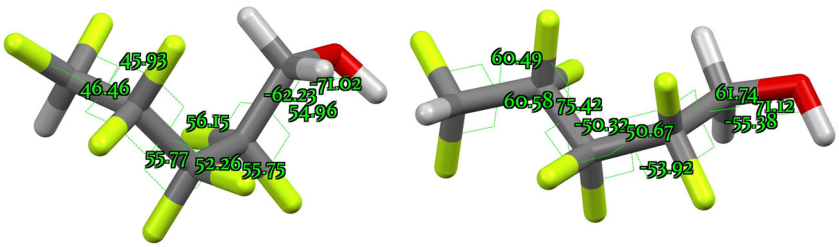

Fig. 10 The two predicted lowest energy conformations of 2,2,3,3,4,4,5,5-octafluoropentan-1-ol exhibiting nine *gauche*-effect orientations, showing torsion angles.

Table 12 RMSD for the various sets of rotamers (ppm) using eqn (3), with values in parentheses using eqn (4)

Set of rotamers	(i)	(ii)	(iii)	(iv)	(v)
RMSD	3.18 (1.65)	3.95 (2.34)	4.49 (2.96)	4.42 (3.10)	3.83 (2.22)

(thf) and acetonitrile both might complex with the 3-coordinate boron atom in difluoro(phenyl)borane to form a 4-coordinate species, these being of particular interest in understanding the mechanisms of amidation using boron catalysts. We calculated the ^{19}F NMR spectra in these two solvents at the ωB97xd/aug-cc-pvdz level, for both the complexed and the free forms (Fig. 11 and 12) with values reported in Table 13.

The combined energies of difluoro(phenyl)borane and one molecule of either thf (tetrahydrofurant) or acetonitrile as solvent can be obtained in two ways. Summing the computed free energies of the individual solute and solvent molecules as model (a) or using the free energy of the combined weakly interacting supermolecule as model (b), with both energies

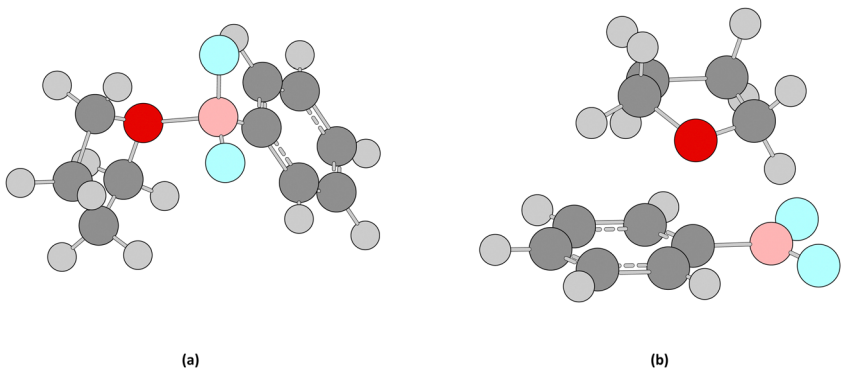

Fig. 11 Structures for (a) the complexed and (b) free difluoro(phenyl)borane in thf, showing the weak dispersion interactions for the two species treated as a supermolecule.

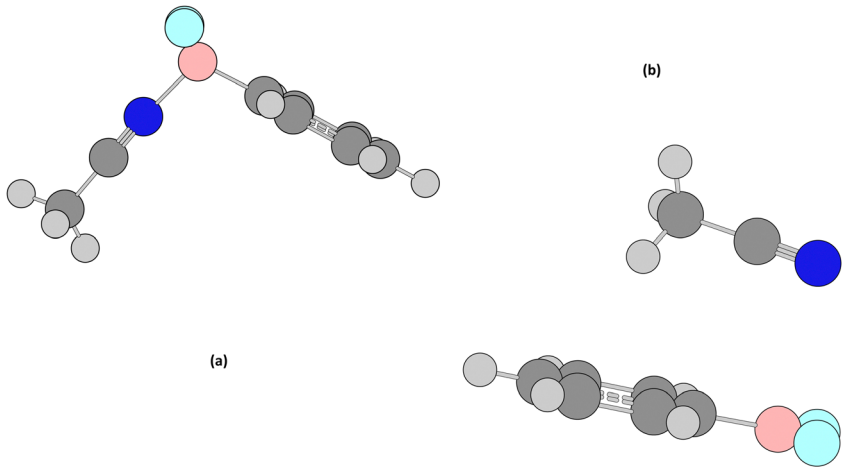

Fig. 12 Structures for (a) the complexed and (b) free difluoro(phenyl)borane in acetonitrile, showing the weak dispersion interactions for the two species treated as a supermolecule.

Table 13 Calculated (eqn (4), ωB97XD/aug-cc-pvdz) and reported ^{19}F NMR chemical shifts for difluoro(phenyl)borane in aprotic coordinating solvents

Solvent	Form	^{19}F chemical shift in ppm (eqn (4))	Reported value
thf	4-Coordinate bound	−155.6	−142[95]
	3-Coordinate unbound	−95.2	
Acetonitrile	4-Coordinate bound	−157.6	−127.9[98]
	3-Coordinate unbound	−96.2	
Pyridine	4-Coordinate bound	−166.8	−154.6
	3-Coordinate unbound	−95.9	
Thiophene	4-Coordinate bound	n/a	—
	3-Coordinate unbound	−93.6	
Sulfolane	4-Coordinate bound	−144.9	—
	3-Coordinate unbound	−96.1	

obtained with a solvent continuum solvation model applied. The first model corresponds approximately to an infinitely dilute solution of the two components and the second to a 0.041 M equimolar solution (equivalent to a standard state of 1 atm@298 K) in which weak dispersion interactions between the two components can reduce the entropy of separation. Since the solvent is in higher concentration (16 M for thf, 31 M for acetonitrile), this also favours the intermolecular equilibrium towards a greater concentration of the solvent-bound 4-coordinate form. The calculated relative free energy of the 4-coordinate species using acetonitrile as solvent is +3.4 kcal mol^{-1} using model (a) and −1.2 kcal mol^{-1} using model (b). Decreasing the free energy of the bound form by −3.9 kcal mol^{-1} to approximate the effect on the equilibrium of the high molar concentration of acetonitrile *via* the expression RTLn(31/0.041), T = 298 K and using model (a), indicates that the resulting concentration of unbound 3-coordinate and of solvent-bound 4-coordinate difluoro(phenyl)borane are approximately equal (populations ∼0.5 : 0.5).

The calculated ^{19}F chemical shifts can now be used as limiting values for the 4-coordinate bound and 3-coordinate unbound molecules to get an experimental estimate of the equilibrium. The shift for the 4-coordinate, formally anionic borate form of difluoro(phenyl)borane, may be predicted to be too negative by ∼6 ppm, as shown by the value for BF_4^- itself (Table 11). Applying this approximate correction suggests that the relative populations of bound/unbound solutes are approximately equal in acetonitrile, deriving from the measured chemical shift of difluoro(phenyl)borane being intermediate between the 3- and 4-coordinate forms in this solvent.

For thf as solvent, combining the calculated corrected limiting chemical shifts for the two forms with the observed value suggests the equilibrium favours 4- over 3-coordinated species by a population ratio of 0.85/0.15. The calculated relative free energy of bound 4-coordinate species for thf as solvent is −0.5 kcal mol^{-1} using model (a), or −4.0 if approximately corrected for the 16 M concentration of thf. This corresponds qualitatively to the measured ^{19}F chemical shift in this solvent distinctly favouring the 4-coordinated form. These results also hint that model (a) might be better for obtaining free energies for weakly interacting separated components in solution. It remains to be established if model (b) might be better for more concentrated solutions of components interacting more strongly through *e.g.* one or more strong hydrogen bonds.

In predictive mode, we investigated three further aprotic coordinating solvents, pyridine, thiophene and sulfolane. Thiophene has no minimum for the bound 4-coordinate isomer, dissociating to the unbound form. With pyridine, the 4-coordinate isomer is now significantly more stable in free energy than the unbound form by −11.7 kcal mol^{-1}. We then measured the ^{19}F and ^{11}B shifts in this solvent, finding the former 13 ppm closer to if not actually at the bound limit than with thf as solvent. The calculated ^{11}B shift (+6.8 ppm) is in close agreement with the measured value (6.3 ppm) which supports the inference that the equilibrium for difluoro-(phenyl)borane indeed favours the fully 4-coordinated form in pyridine and which is supported by the energy difference of −11.7 kcal mol^{-1} between it and the unbound 3-coordinate form.

Sulfolane is predicted to be similar to thf, with the bound form 0.34 kcal mol^{-1} less stable than the unbound separated components, but is favoured if a correction (3.0 kcal mol^{-1}) for the higher molar concentration of the solvent (6.6 M) is applied.

Further insight was obtained by searching for crystal structures containing the sub-structure C–BF–X (X = O, N) and analysing seven such structures, five of which form an intramolecular B–X bond and two of which are sterically inhibited from doing so (Fig. 11 and 12). The former set are examples of potential intramolecular equilibria in which a boron atom could display either a tri- or a four-coordinated form.[121,142–146] These seven molecules are shown in Fig. 13 and the chemical shift values in Table 14.

Of the species shown in Fig. 11, ZICMIJ has no formal stationary point for a 3-coordinate species, but it does appear as an inflexion in the energy surface typical of a "hidden intermediate" and can be estimated to be 13.7 kcal mol^{-1} higher in free energy than the 4-coordinate isomer. True intramolecular 3-coordinate forms can be located as formal stationary points for CUJSEG (+40.7 kcal mol^{-1}), LOCNOJ (+32.3 kcal mol^{-1}), CICPEM (+23.5 kcal mol^{-1}) and NUJQUE (+19.3 kcal mol^{-1}), with their free energies relative to the 4-coordinate forms shown parentheses. The values suggest that in all cases the 4-coordinate form is the only one with a significant population (1.00) in solution.

The reported ^{19}F shift for the methylamino substituted NUJQUE (and of its octylamino derivative) of −54.5 ppm (compounds **15** and **16** in the article,[148] ^{19}F nmr reference not stated) is anomalous in comparison with the other compounds shown in Fig. 11 and also with the predicted ^{19}F. The ^{11}B shifts for NUJQUE reported as −15 ppm agree well with a calculated value

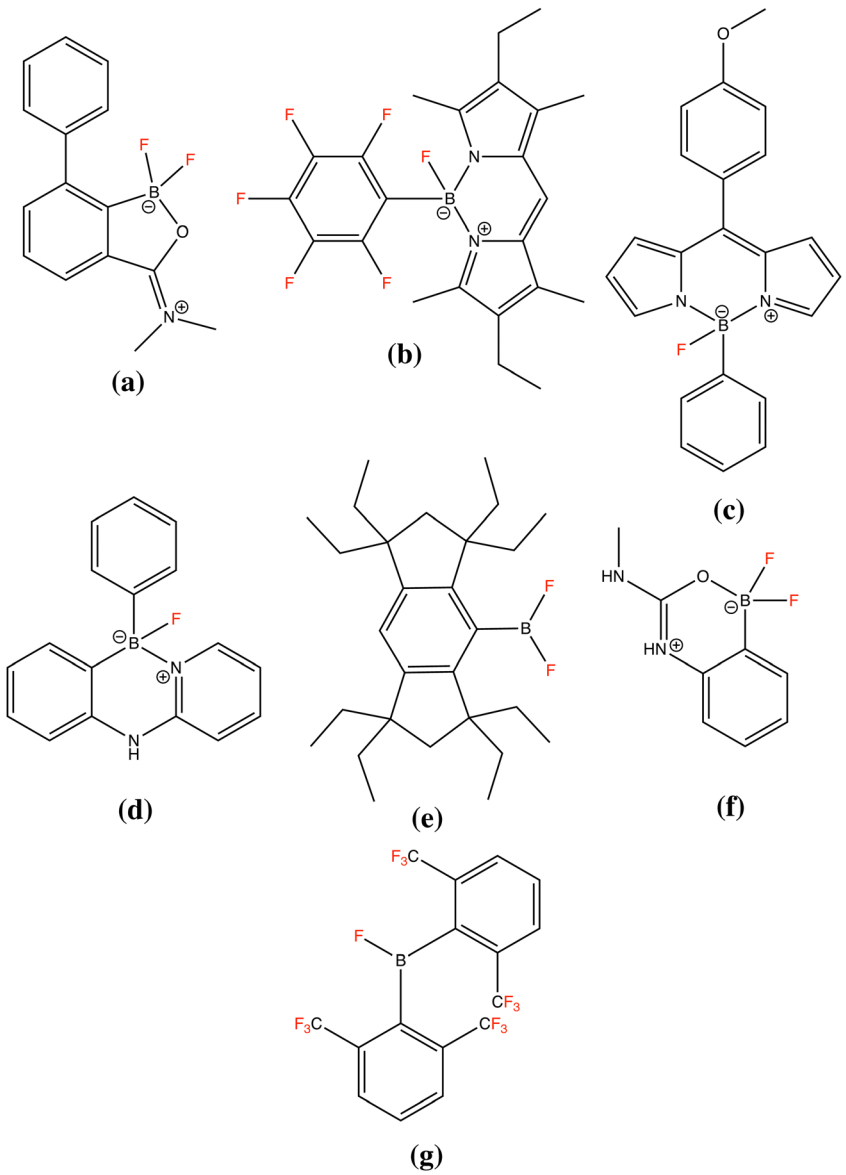

Fig. 13 Structures and Cambridge Refcode identifier of the test set for 4/3-coordinate-boron equilibria. (a) ZICMIJ, (b) CUJSEG, (c) LOCNOJ, (d) CICPEM, (e) UYELAN, (f) NUJQUE and (g) TAKWIO. The crystal structures can be found in the data repository.[147]

Table 14 Experimental ^{19}F shifts in ppm, with calculated values (eqn (4), ωB97XD/aug-cc-pvdz) for the test set shown in Fig. 13

Compound	Experimental	4-Coordinate form	3-Coordinate form
ZICMIJ	−149.1[142]	−154.7	−82.8
CUJSEG	−163.8[145]	−171.9	−75.3
LOCNOJ	−161.84[146]	−164.2	−92.3
CICPEM	−165.1[144]	−164.3	−65.2
NUJQUE	−54.5[148]	−137.8	−90.1
UYELAN	−56.4[149]	−134.0	−58.1
TAKWIO	−56.6 (CF_3), −11.0 (BF)[150]	−57.0, −136.9	−58.0, −12.9

of −13.3 ppm using $B(OMe)_3$ as reference, indicating the molecule probably has the constitution indicated. This in turn suggests the unstated ^{19}F reference for the measured shift[148] may not be $CFCl_3$ but CF_3H (calc. −57.5) or more probably trifluoroacetic acid (calc. −60.9). Assuming the latter, re-referenced with respect to $CFCl_3$ the measured value for NUJQUE emerges as −131.5 ppm, in reasonable agreement with the predicted value for a 4-coordinate boron species.

UYELAN and TAKWIO are examples of fluoroboranes in which steric hindrance inhibits formation of a 4-coordinate form. For UYELAN, 4-coordination *via* the oxygen of thf results in a species that is 8.6 kcal mol^{-1} higher than the individual dissociated components, and so this form is predicted to have no significant population in solution. TAKWIO is also sterically hindered and the 4-coordinate form in thf is 11.1 kcal mol^{-1} higher in free energy than the non-coordinated form, again unpopulated. The ^{19}F chemical shifts are all well predicted as 3-coordinate for these systems, suggesting that predictive NMR can be used to estimate positions of 3-/4-coordinate dynamic equilibria where they might occur.

5 Conclusions

^{19}F NMR is a powerful tool that can used for the structure determination of fluorinated molecules. We provide herein computational tools to help estimate ^{19}F chemical shifts using reasonable computer resources and with an accuracy of 3–4 ppm or better, providing an additional asset to the synthesis or the study of catalytic mechanisms in which fluorine is exploited as an analytic probe.

Author contributions

A. S. Dumon provided methodology, formal analysis, investigation, visualisation, data curation and writing. H. S. Rzepa provided conceptualisation and project administration, data curation and writing. R. Procter provided chemical synthesis and with the other authors analysis, review and editing.

Conflicts of interest

There are no conflicts to declare.

Acknowledgements

We acknowledge the EPSRC for grants EP/T030488/1, EP/T030534/1, EP/T030658/1, EP/T030666/1. We thank Dr Chris Edge for invaluable statistical advice.

References

1 G. E. Totten and D. S. MacKenzie, *Handbook of Aluminum*, Dekker, 2003, vol. 2.
2 J. Wang, M. Sánchez-Roselló, J. L. Aceña, C. del Pozo, A. E. Sorochinsky, S. Fustero, V. A. Soloshonok and H. Liu, *Chem. Rev.*, 2014, **114**, 2432–2506.
3 J. T. Moore and C. C. Lu, *J. Am. Chem. Soc.*, 2020, **142**, 11641–11646.
4 L. I. Khusainova, L. O. Khafizova, T. V. Tyumkina and U. M. Dzhemilev, *Russ. J. Gen. Chem.*, 2016, **86**, 1438–1441.
5 N. Murakami, M. Yoshida, T. Yoshino and S. Matsunaga, *Chem. Pharm. Bull.*, 2018, **66**, 51–54.
6 T. Furuya, A. S. Kamlet and T. Ritter, *Nature*, 2011, **473**, 470–477.
7 H. Robatjazi, J. L. Bao, M. Zhang, L. Zhou, P. Christopher, E. A. Carter, P. Nordlander and N. J. Halas, *Nat. Catal.*, 2020, **3**, 564–573.
8 Y.-C. Ning and R. R. Ernst, *Structural Identification of Organic Compounds with Spectroscopic Techniques*, Wiley-VCH, 2005.
9 T. D. W. Claridge, *High-Resolution NMR Techniques in Organic Chemistry*, Elsevier Science, 2016.
10 C. P. Rosenau, B. J. Jelier, A. D. Gossert and A. Togni, *Angew. Chem., Int. Ed.*, 2018, **57**, 9528–9533.
11 S. Sirirungruang, O. Ad, T. M. Privalsky, S. Ramesh, J. L. Sax, H. Dong, E. E. K. Baidoo, B. Amer, C. Khosla and M. C. Y. Chang, *Nat. Chem. Biol.*, 2022, **18**, 886–893.
12 A. M. Ruppert, M. Jędrzejczyk, O. Sneka-Płšatek, N. Keller, A. S. Dumon, C. Michel, P. Sautet and J. Grams, *Green Chem.*, 2016, **18**, 2014–2028.
13 A. S. Dumon, T. Wang, J. Ibañez, A. Tomer, Z. Yan, R. Wischert, P. Sautet, M. Pera-Titus and C. Michel, *Catal. Sci. Technol.*, 2018, **8**, 611–621.
14 C.-H. Chan, F. Poignant, M. Beuve, E. Dumont and D. Loffreda, *J. Phys. Chem. Lett.*, 2019, **10**, 1092–1098.
15 M. Dhifallah, M. Iachella, A. Dhouib, F. Di Renzo, D. Loffreda and H. Guesmi, *J. Phys. Chem. C*, 2019, **123**, 4892–4902.
16 H. S. Rzepa, S. Arkhipenko, E. Wan, M. T. Sabatini, V. Karaluka, A. Whiting and T. D. Sheppard, *J. Org. Chem.*, 2018, **83**, 8020–8025.
17 S. V. Fedorov and L. B. Krivdin, *J. Fluorine Chem.*, 2020, **238**, 109625.
18 L. B. Krivdin, *Russian Chem. Rev.*, 2020, **89**, 104.
19 H. Fukaya and T. Ono, *J. Comput. Chem.*, 2004, **25**, 51–60.
20 W. Adcock, D. Lünsmann, J. E. Peralta and R. H. Contreras, *Magn. Reson. Chem.*, 1999, **37**, 167–172.
21 J.-D. Chai and M. Head-Gordon, *Phys. Chem. Chem. Phys.*, 2008, **10**, 6615–6620.

22 W. C. Isley, A. K. Urick, W. C. K. Pomerantz and C. J. Cramer, *Mol. Pharmaceutics*, 2016, **13**, 2376–2386.
23 H. P. Ebrahimi and M. Tafazzoli, *Concepts Magn. Reson., Part A*, 2012, **40**, 192–204.
24 J.-H. Yang, L. A. Clark, G. J. Ray, Y. J. Kim, H. Du and R. Q. Snurr, *J. Phys. Chem. B*, 2001, **105**, 4698–4708.
25 J. C. B. Dietschreit, A. Wagner, T. A. Le, P. Klein, H. Schindelin, T. Opatz, B. Engels, U. A. Hellmich and C. Ochsenfeld, *Angew. Chem., Int. Ed.*, 2020, **59**, 12669–12673.
26 P. Gao, J. Zhang and H. Chen, *Int. J. Quantum Chem.*, 2021, **121**, e26482.
27 E. Benassi, *J. Comput. Chem.*, 2022, **43**, 170–183.
28 *Organic Chemistry Database*, **https://organicchemistrydata.org/**.
29 *Reaxys*, **https://www.reaxys.com/**.
30 C. Cave-Ayland, M. J. Bearpark, C. Romain and H. S. Rzepa, *J. Opensource Software*, 2022, **70**, 3824.
31 M. J. Harvey, A. Mclean and H. S. Rzepa, *J. Cheminformatics*, 2017, **9**, 4.
32 S. Miertuň, E. Scrocco and J. Tomasi, *Chem. Phys.*, 1981, **55**, 117–129.
33 S. Miertus and J. Tomasi, *Chem. Phys.*, 1982, **65**, 239–245.
34 J. L. Pascual-ahuir, E. Silla and I. Tuñon, *J. Comput. Chem.*, 1994, **15**, 1127–1138.
35 A. D. Becke, *J. Chem. Phys.*, 1988, **88**, 1053–1062.
36 C. Lee, W. Yang and R. G. Parr, *Phys. Rev. B*, 1988, **37**, 785–789.
37 M. J. Frisch, M. Head-Gordon and J. A. Pople, *Chem. Phys. Lett.*, 1990, **166**, 275–280.
38 M. J. Frisch, M. Head-Gordon and J. A. Pople, *Chem. Phys. Lett.*, 1990, **166**, 281–289.
39 M. Head-Gordon, J. A. Pople and M. J. Frisch, *Chem. Phys. Lett.*, 1988, **153**, 503–506.
40 S. Sæbø and J. Almlöf, *Chem. Phys. Lett.*, 1989, **154**, 83–89.
41 M. Head-Gordon and T. Head-Gordon, *Chem. Phys. Lett.*, 1994, **220**, 122–128.
42 T. H. Dunning, *J. Chem. Phys.*, 1989, **90**, 1007–1023.
43 F. Weigend and R. Ahlrichs, *Phys. Chem. Chem. Phys.*, 2005, **7**, 3297–3305.
44 F. Weigend, *Phys. Chem. Chem. Phys.*, 2006, **8**, 1057–1065.
45 B. P. Pritchard, D. Altarawy, B. Didier, T. D. Gibsom and T. L. Windus, *J. Chem. Inf. Model.*, 2019, **59**, 4814–4820.
46 D. Feller, *J. Comput. Chem.*, 1996, **17**, 1571–1586.
47 K. L. Schuchardt, B. T. Didier, T. Elsethagen, L. Sun, V. Gurumoorthi, J. Chase, J. Li and T. L. Windus, *J. Chem. Inf. Model.*, 2007, **47**, 1045–1052.
48 F. Jensen, *J. Chem. Theory Comput.*, 2015, **11**, 132–138.
49 S. Grimme, S. Ehrlich and L. Goerigk, *J. Comput. Chem.*, 2011, **32**, 1456–1465.
50 F. London, *J. Phys. Radium*, 1937, **8**, 397–409.
51 R. McWeeny, *Phys. Rev.*, 1962, **126**, 1028–1034.
52 R. Ditchfield, *Mol. Phys.*, 1974, **27**, 789–807.
53 K. Wolinski, J. F. Hinton and P. Pulay, *J. Am. Chem. Soc.*, 1990, **112**, 8251–8260.
54 M. Klaupp, O. L. Malkina and V. G. Malkin, *J. Comput. Chem.*, 1999, **20**, 1304–1313.
55 A. Dumon, H. S. Rzepa, C. Alamillo-Ferrer, J. Bures, R. Procter, T. D. Sheppard and A. Whiting, *Imperial College Research Data Repository*, 2021, DOI: **10.14469/hpc/8772**.
56 Z. Cong, T. Kurahashi and H. Fujii, *J. Am. Chem. Soc.*, 2012, **134**, 4469–4472.
57 D. Velayutham, K. Jayaraman, K. Kulangiappar, N. Ilayaraja, Y. R. Babu, P. S. Rao, S. N. Reddy, K. V. Babu and M. Noel, *J. Fluorine Chem.*, 2006, **127**, 1111–1118.
58 H. Schneider, A. Hock, A. D. Jaeger, D. Lentz and U. Radius, *Eur. J. Inorg. Chem.*, 2018, 4031–4043.
59 D. A. Ellis, J. W. Martin, D. C. G. Muir and S. A. Mabury, *Anal. Chem.*, 2000, **72**, 726–731.
60 N. M. Hein, F. S. Pick and M. D. Fryzuk, *Inorg. Chem.*, 2017, **56**, 14513–14523.
61 A. Ribeiro and M. Glen, *J. Mag. Res., Ser. A*, 1994, **107**, 158–166.
62 H. Nakai, K. Jeong, T. Matsumoto and S. Ogo, *Organometallics*, 2014, **33**, 4349–4352.
63 D. D. L. Jones, I. Douair, L. Maron and C. Jones, *Angew. Chem., Int. Ed.*, 2021, **60**, 7087–7092.
64 S. Ando and T. Matsuura, *Mag. Reson. Chem.*, 1995, **33**, 639–645.
65 P. Xu, P. López-Rojas and T. Ritter, *J. Am. Chem. Soc.*, 2021, **143**, 5349–5354.
66 A. Foris, *Mag. Reson. Chem.*, 2004, **42**, 534–555.
67 A. Bakhoda, O. E. Okoromoba, C. Greene, M. R. Boroujeni, J. A. Bertke and T. H. Warren, *J. Am. Chem. Soc.*, 2020, **142**, 18483–18490.
68 J.-P. Dietz, B. P. Derstine, D. Ferenc, E. T. Crawford, A. J. Arduengo III, B. F. Gupton, D. T. McQuade and T. Opatz, *Eur. J. Org. Chem.*, 2019, 5519–5526.
69 F.-L. Zeng, K. Sun, X.-L. Chen, X.-Y. Yuan, S.-Q. He, Y. Liu, Y.-Y. Peng, L.-B. Qu, Q.-Y. Lv and B. Yu, *Adv. Synth. Catal.*, 2019, **361**, 5176–5181.
70 A. Aydogan, D. J. Coady, S. K. Kim, A. Akar, C. Bielawski, M. Marquez and J. Sessler, *Angew. Chem., Int. Ed.*, 2008, **47**, 9648–9652.
71 F. Weigert, *J. Fluorine Chem.*, 1990, **46**, 375–384.
72 T. Mohy El Dine, O. Sadek, E. Gras and D. M. Perrin, *Chem. – Eur. J.*, 2018, **24**, 14933–14937.
73 D. Dunlop, J. Pinkas, M. Horáček, N. Žilková and M. Lamač, *Dalton Trans.*, 2020, **49**, 2771–2775.
74 L. P. Press, A. J. Kosanovich, B. J. McCulloch and O. V. Ozerov, *J. Am. Chem. Soc.*, 2016, **138**, 9487–9497.
75 M. Baya, D. Joven-Sancho, P. J. Alonso, J. Orduna and B. Menjón, *Angew. Chem., Int. Ed.*, 2019, **58**, 9954–9958.
76 A. B. Grommet, J. L. Bolliger, C. Browne and J. R. Nitschke, *Angew. Chem., Int. Ed.*, 2015, **54**, 15100–15104.
77 W. Jud, S. Maljuric, C. O. Kappe and D. Cantillo, *Org. Lett.*, 2019, **21**, 7970–7975.
78 A. Zweig, R. G. Fischer and J. E. Lancaster, *J. Org. Chem.*, 1980, **45**, 3597–3603.
79 K. L. Bamford, S. S. Chitnis, Z.-W. Qu and D. W. Stephan, *Chem. – Eur. J.*, 2018, **24**, 16014–16018.
80 O. Koleda, T. Broese, J. Noetzel, M. Roemelt, E. Suna and R. Francke, *J. Org. Chem.*, 2017, **82**, 11669–11681.

81 C.-P. Zhang, J. Cai, C.-B. Zhou, X.-P. Wang, X. Zheng, Y.-C. Gu and J.-C. Xiao, *Chem. Commun.*, 2011, **47**, 9516–9518.
82 S. Y. Erdyakov, A. V. Ignatenko, M. E. Gurskii and Y. N. Bubnov, *Mendeleev Commun.*, 2007, **17**, 271–273.
83 S. Fantasia, J. M. Welch and A. Togni, *J. Org. Chem.*, 2010, **75**, 1779–1782.
84 C. Colomban, E. V. Kudrik, P. Afanasiev and A. B. Sorokin, *J. Am. Chem. Soc.*, 2014, **136**, 11321–11330.
85 Z.-Y. Liu and S. P. Cook, *Org. Lett.*, 2021, **23**, 808–813.
86 M. E. Zick, J.-H. Lee, M. I. Gonzalez, E. O. Velasquez, A. A. Uliana, J. Kim, J. R. Long and P. J. Milner, *J. Am. Chem. Soc.*, 2021, **143**, 1948–1958.
87 T. Yang, H. Lu, Y. Shu, Y. Ou, L. Hong, C.-T. Au and R. Qiu, *Org. Lett.*, 2020, **22**, 827–831.
88 F. Le Vaillant, E. J. Reijerse, M. Leutzsch and J. Cornella, *J. Am. Chem. Soc.*, 2020, **142**, 19540–19550.
89 N. Ichiishi, A. J. Canty, B. F. Yates and M. S. Sanford, *Org. Lett.*, 2013, **15**, 5134–5137.
90 T. Remarchuk and E. Corey, *Tetrahedron Lett.*, 2018, **59**, 2256–2259.
91 P. Tang, T. Furuya and T. Ritter, *J. Am. Chem. Soc.*, 2010, **132**, 12150–12154.
92 M. K. Cybulski, C. J. E. Davies, J. P. Lowe, M. F. Mahon and M. K. Whittlesey, *Inorg. Chem.*, 2018, **57**, 13749–13760.
93 G. Meißner, M. Feist, T. Braun and E. Kemnitz, *J. Organomet. Chem.*, 2017, **847**, 234–241.
94 G. Berionni, H. Kurouchi, L. Eisenburger and H. Mayr, *Chem. – Eur. J.*, 2016, **22**, 11196–11200.
95 M. M. Shmakov, S. A. Prikhod'ko, V. V. Bardin and N. Y. Adonin, *Mendeleev Commun.*, 2018, **28**, 369–371.
96 S. Liu, H. Liu, S. Liu, Z. Lu, C. Lu, X. Leng, Y. Lan and Q. Shen, *J. Am. Chem. Soc.*, 2020, **142**, 9785–9791.
97 K. Oisaki, D. Zhao, M. Kanai and M. Shibasaki, *J. Am. Chem. Soc.*, 2006, **128**, 7164–7165.
98 B. J. Kim and D. S. Matteson, *Angew. Chem., Int. Ed.*, 2004, **43**, 3056–3058.
99 M. Kol, S. Rozen and E. Appelman, *J. Am. Chem. Soc.*, 1991, **113**, 2648–2651.
100 H. J. Frohn and W. Pahlmann, *J. Fluorine Chem.*, 1984, **24**, 219–232.
101 N. V. Lebedev, V. V. Berenblit, P. E. Troichanskaya and V. A. Gubanov, *Russian J. App. Chem.*, 2009, **82**, 449–455.
102 J. Mizukado, Y. Matsukawa, H. dao Quan, M. Tamura and A. Sekiya, *J. Fluorine Chem.*, 2006, **127**, 79–84.
103 H. Bürger and S. Sommer, *J. Chem. Soc., Chem. Commun.*, 1991, 456–458.
104 H. Frohn and R. Nielinger, *J. Fluorine Chem.*, 1996, **77**, 143–146.
105 X. Jia, X. Zhou, H. Quan, M. Tamura and A. Sekiya, *J. Fluorine Chem.*, 2011, **132**, 1188–1193.
106 T. A. Shaler and T. H. Morton, *J. Am. Chem. Soc.*, 1991, **113**, 6771–6779.
107 N. O. Andrella, N. Xu, B. M. Gabidullin, C. Ehm and R. T. Baker, *J. Am. Chem. Soc.*, 2019, **141**, 11506–11521.
108 P. S. Bhadury, M. Pandey and D. K. Jaiswal, *J. Fluorine Chem.*, 1995, **73**, 185–187.
109 S. Hämmerling, G. Thiele, S. Steinhauer, H. Beckers, C. Müller and S. Riedel, *Angew. Chem., Int. Ed.*, 2019, **58**, 9807–9810.
110 M. Ahrens, G. Scholz, T. Braun and E. Kemnitz, *Angew. Chem., Int. Ed.*, 2013, **52**, 5328–5332.
111 J. Guang, R. Hopson, P. G. Williard, M. Fujiu, K. Negishi and K. Mikami, *J. Org. Chem.*, 2016, **81**, 5922–5928.
112 S. Wilken, M. Treskow, J. Scheers, P. Johansson and P. Jacobsson, *RSC Adv.*, 2013, **3**, 16359–16364.
113 S. A. Lermontov, L. L. Ushakova and N. V. Kuryleva, *J. Fluorine Chem.*, 2008, **129**, 332–334.
114 B. M. Kraft, R. J. Lachicotte and W. D. Jones, *J. Am. Chem. Soc.*, 2001, **123**, 10973–10979.
115 M. Talavera, G. Meiner, S. G. Rachor and T. Braun, *Chem. Commun.*, 2020, **56**, 4452–4455.
116 L. A. Bischoff, J. Riefer, R. Wirthensohn, T. Bischof, R. Bertermann, N. V. Ignatev and M. Finze, *Chem. – Eur. J.*, 2020, **26**, 13615–13620.
117 S. L. Guillot, A. Peña-Hueso, M. L. Usrey and R. J. Hamers, *J. Electrochem. Soc.*, 2017, **164**, A1907–A1917.
118 D. G. Altman and J. M. Bland, *J. R. Stat. Soc. Ser. D*, 1983, **32**, 307–317.
119 A. Dumon, Imperial College Research Data Repository, 2021, DOI: **10.14469/hpc/9915**.
120 F. Rauch, S. Fuchs, A. Friedrich, D. Sieh, I. Krummenacher, H. Braunschweig, M. Finze and T. B. Marder, *Chem. – Eur. J.*, 2020, **26**, 12794–12808.
121 A. G. Crawford, Z. Liu, I. A. I. Mkhalid, M.-H. Thibault, N. Schwarz, G. Alcaraz, A. Steffen, J. C. Collings, A. S. Batsanov, J. A. K. Howard and T. B. Marder, *Chem. – Eur. J.*, 2012, **18**, 5022–5035.
122 C. R. Wade, H. Zhao and F. P. Gabbaï, *Chem. Commun.*, 2010, **46**, 6380–6381.
123 A. L. Gott, W. E. Piers, J. L. Dutton, R. McDonald and M. Parvez, *Organometallics*, 2011, **30**, 4236–4249.
124 J. Légaré Lavergne, A. Jayaraman, L. C. Misal Castro, E. Rochette and F.-G. Fontaine, *J. Am. Chem. Soc.*, 2017, **139**, 14714–14723.
125 K. Durka, M. Urban, M. Dąbrowski, P. Jankowski, T. Klił and S. Luliłżski, *ACS Omega*, 2019, **4**, 2482–2492.
126 S. Jin, H. T. Dang, G. C. Haug, R. He, V. D. Nguyen, V. T. Nguyen, H. D. Arman, K. S. Schanze and O. V. Larionov, *J. Am. Chem. Soc.*, 2020, **142**, 1603–1613.
127 A. Dumon, Imperial College Research Data Repository, 2021, DOI: **10.14469/hpc/9649**.
128 C. R. Groom, I. J. Bruno, M. P. Lightfoot and S. C. Ward, *Acta Crystallogr., Sect. B: Struct. Sci., Cryst. Eng. Mater.*, 2016, **72**, 171–179.
129 K. Monde, N. Miura, M. Hashimoto, T. Taniguchi and T. Inabe, *J. Am. Chem. Soc.*, 2006, **128**, 6000–6001.
130 Y. S. Sokeirik, H. Mori, M. Omote, K. Sato, A. Tarui, I. Kumadaki and A. Ando, *Org. Lett.*, 2007, **9**, 1927–1929.
131 A. Berkessel, S. S. Vormittag, N. E. Schlörer and J.-M. Neudörfl, *J. Org. Chem.*, 2012, **77**, 10145–10157.
132 D.-J. Barrios Antùonez, M. D. Greenhalgh, A. C. Brueckner, D. M. Walden, P. Elias-Rodriguez, P. Roberts, B. G. Young,

T. H. West, A. M. Z. Slawin, P. Ha-Yeon Cheong and A. D. Smith, *Chem. Sci*, 2019, **10**, 6162–6173.
133 C. Sperandio, J. Rodriguez and A. Quintard, *Chem. Sci.*, 2020, **11**, 1629–1635.
134 A. Rudnichenko, V. Timoshenko, A. Chernega, A. Nesterenko and Y. Shermolovich, *J. Fluorine Chem.*, 2004, **125**, 1351–1356.
135 K. Funabiki, H. Iwata, Y. Yano, Y. Kubota and M. Matsui, *Org. Chem. Front.*, 2015, **2**, 369–371.
136 A. Maity, A. Sarkar, B. N. S. Bhaktha and S. K. Patra, *New J. Chem.*, 2020, **44**, 14650–14661.
137 D. E. Arkhipov, A. V. Lyubeshkin, A. D. Volodin and A. A. Korlyukov, *Mendeleev Commun.*, 2020, **30**, 103–105.
138 P. A. Slepukhin, V. I. Filyakova and V. N. Charushin, *J. Struct. Chem.*, 2012, **53**, 1011–1012.
139 K. I. Pashkevich, D. V. Sevenard, O. G. Khomutov, O. V. Shishkin and E. V. Solomovich, *Russ. Chem. Bull.*, 1999, **48**, 359–363.
140 A. Dumon, Imperial College Research Data Repository, 2021, DOI: **10.14469/hpc/10504**.
141 A. N. Bootsma and S. Wheeler, Popular Integration Grids Can Result in Large Errors in DFT-Computed Free Energies, *ChemRxiv*, 2019, DOI: **10.26434/chemrxiv.8864204**.
142 J. D. Kirkham, R. J. Butlin and J. P. A. Harrity, *Angew. Chem., Int. Ed.*, 2012, **51**, 6402–6405.
143 D. Pla, O. Sadek, S. Cadet, B. Mestre-Voegtl and E. Gras, *Dalton Trans.*, 2015, **44**, 18340–18346.
144 K. Yang, G. Zhang and Q. Song, *Chem. Sci.*, 2018, **9**, 7666–7672.
145 C. Bonnier, W. E. Piers, A. Al-Sheikh Ali, A. Thompson and M. Parvez, *Organometallics*, 2009, **28**, 4845–4851.
146 Z. Wang, C. Cheng, Z. Kang, W. Miao, Q. Liu, H. Wang and E. Hao, *J. Org. Chem.*, 2019, **84**, 2732–2740.
147 A. Dumon, Imperial College Research Data Repository, 2021, DOI: **10.14469/hpc/10243**.
148 M. P. Hughes and B. D. Smith, *J. Org. Chem.*, 1997, **62**, 4492–4499.
149 T. Murosaki, S. Kaneda, R. Maruhashi, K. Sadamori, Y. Shoji, K. Tamao, D. Hashizume, N. Hayakawa and T. Matsuo, *Organometallics*, 2016, **35**, 3397–3405.
150 K. Samigullin, Y. Soltani, H.-W. Lerner, M. Wagner and M. Bolte, *Acta Crystallogr., Sect. C: Struct. Chem.*, 2016, **72**, 189–197.